

Learning from Interpolated Images using Neural Networks for Digital Forensics

Yizhen Huang
Computer Sciences Department
University of Wisconsin-Madison
huang.yizhen@gmail.com

Na Fan
Department of Electronic Engineering
East China Normal University
fanna.cn@gmail.com

Abstract

Interpolated images have data redundancy, and special correlation exists among neighboring pixels, which is a crucial clue in digital forensics. We design a neural network based framework to approximate the stylized computational rules of interpolation algorithms for learning statistical inter-pixel correlation of interpolated images. The interpolation process is cognized from the interpolation results. Experiments are carried out on camera built-in Color Filter Array interpolation and super resolution. Three classifiers are trained to classify image interpolation algorithms, identify source cameras and uncover digital forgeries. Like the Wiener attack in watermarking, the special correlation can be reduced or transferred it to another image by our learned network.

1. Introduction

The detection of doctored photos (e.g. Figure 1) is becoming increasingly interested by the computer vision community. Due to the intrinsic structure of digital color cameras, digital photos are subjected to a sequence of image processing pipelines before their acquisition by end users. Such traces left therein by cameras are important, since they are different from photo post-processing manipulation and malicious forgeries (see [1-2] for surveys).

One of the most widely used traces is the Demosaicking Inter-Pixel Correlation (DIPC). For example, Kharrazi et al. [3] tried to identify source cameras in Color Filter Array (CFA) configuration by a feature-based approach. It was extended by Bayram et al. [4], who defined a set of image characteristics and applied a Support Vector Machine (SVM) based multi-class classifier to determine the originating digital camera. Popescu et al. [5] modeled the DIPC of a pixel as a linear correlation of its 8-connectivity immediate neighboring pixels and solved this model with the Expectation / Maximization algorithm, which is useful for image forgery detection. As an amelioration, Celiktutan et al. [6] explored feature fusion and decision fusion schemes on a larger category of features.



Figure 1. Iranian missile test photos: (a) is real, while (b) is accused of being altered by Iran to exaggerate their military power.

Long and Huang [7-8] modeled the problem using a quadratic form and discovered that, scene correlation generally distributes evenly over Principal Components Analysis (PCA) space of the quadratic coefficient matrix while DIPC clusters at dimensions corresponding to large eigenvalues. If the quadratic coefficient matrix is considered as features, this model is appropriate to be viewed as feature-based. Swaminathan et al. [9] studied demosaicking artifacts using an analysis-by-synthesis method: An image is divided into 3 regions according to gradient features in a local neighborhood and then, interpolation coefficients are estimated via Singular Value Decomposition (SVD) for each region and each color band, separately. After that all candidate sampled CFA patterns are re-interpolated and the one minimizing the difference between estimated final image and actual image produced by the camera is chosen. It becomes an analytical approach, since it employs SVD, rather than directing the 9 sets of linear equations corresponding to the 3 types of regions and RGB color channels to Support Vector Machines (SVMs) or Neural Networks (NNs) for classification. Analogously, if the quadratic form in [8] was resolved, it would bring about another analytical approach.

We propose an NN-based framework to solve such problem in this paper. It is to be noted that, while some previous work such as [7,8,10] also applied NN for DIPC-based digital forensics, it is only used as a classifier for non-linear flexibility. In contrast, we directly employ a special kind of NNs, namely Compositional Pattern-Producing Networks (CPPNs) to estimate the unknown pixel interrelationship within a more general framework, which makes it different from existing work. The proposed method is also feasible to be applied to classify real commercial cameras and other interpolation algorithms such as image super-resolution.

The rest of the manuscript is organized as follows: Section 2 interprets demosaicking algorithms from a new perspective; Section 3 details the proposed method; Section 4 discusses experimental results and finally, Section 5 is the concluding remark and some possible future work.

2. Demosaicking Revisited

Owing to technological constraints, most commercial digital still color cameras use a single CCD or CMOS electronic sensor overlaid with a CFA in a way that, each sample point captures just one sample of the color spectrum and the other colors must be interpolated. This interpolation process is called CFA interpolation, a.k.a. demosaicking, which has been extensively study in the last two decades. We refer the reader to [11] as a survey. There are full-color CMOS cameras, such as the Sigma SD9 / SD10 Single Lens Reflex camera equipped with the Foveon X3 capture technology that absorbs each color spectrum with layered sensor stack in silicon wafer. But they are very expensive and not suitable for mass production in commercial use.

The CFA commonly embedded in most digital cameras are the Bayer CFA [12], the CMYG CFA (Cyan, Magenta, Yellow and Green) and the CMYK CFA (Cyan, Magenta, Yellow and Key) [2].

Demosaicking algorithms concerned in our experiments are revisited from the perspective of computational rules:

(1) Linear: The simplest methods for demosaicking are kernel-based linear filtering operations that act on each channel independently, such as the bilinear and bicubic interpolation. If hue is defined as the difference between a chrominance component (red or blue) and the luminance component (green) (denoted as the subtractive hue), the Constant Hue-Based (CHB) [13] interpolation can also be regarded as a channel dependent linear filter.

(2) Multiplicative: If hue is defined as the ratio between a chrominance component and the luminance component (denoted as the ratio hue), the CHB interpolation becomes multiplicative. In order to better depict such quantitative relation, the ratio hues and pixel value logarithms of all pixels from the correlated pixel set are served as auxiliary inputs to NNs. Interestingly, the square of our ratio hue is called RGB pairs energy ratio in [5] and is said to be important in forensics feature selection, as it is used in the process of white point correction that is an integral part of a camera pipeline. Notwithstanding the fact that, linear or multiplicative demosaicking filters are rarely in use alone by modern commercial cameras, they are of fundamental importance to our framework since many contemporary methods used them as a module or an initialization step for further iteration or refinement.

(3) Gradient-based adaptive: The gradient-based method was firstly proposed by Laroche et al. [14] and used in the Kodak DCS200 camera. It preserves edge information by preventing interpolation across edges in the luminance channel utilizing chrominance gradients: second-order

derivatives along the horizontal and vertical directions are computed as gradients. If the horizontal gradient is larger than the vertical one, suggesting a possible horizontal edge, interpolation is done vertically and vice versa. One of its variations is the Threshold-Based Variable Number of Gradients (TBVNG) method [15], which uses directional information and adds the ability to use multiple directions. To learn this adaptive process, an image patch orientation-independent NN computation is designed by choosing the NN output closest to the known interpolation result among inputs with 0° , 90° , 180° , 270° rotation of the correlated pixel patch and its mirror image: $NN'(I0)=NN'(I90)=NN'(I180)=NN'(I270)=NN'(I*0)=NN'(I*90)=NN'(I*180)=NN'(I*270)=T \pm \min\{|NN(I0)-T|, |NN(I90)-T|, |NN(I180)-T|, |NN(I270)-T|, |NN(I*0)-T|, |NN(I*90)-T|, |NN(I*180)-T|, |NN(I*270)-T|\}$, where $I0$ is the patch of correlated pixels, $I*0$ is its mirror, the subscripts 0, 90, 180, 270 note as rotation angles, NN' is the enhanced orientation-independent NN, \pm is determined by the sign of the optimal $NN(I)-T$, and T is the target value i.e. the known interpolation result. As our task is to cognize interpolation process from interpolation results, the interpolation result is always known no matter in NN training or simulation.

(4) Learning-based: It has been well acknowledged that demosaicking is a highly nonlinear process. NN is capable of learning complex nonlinear functions, and produces excellent results in high-frequency regions. Go et al. [16] applied three-layer feed-forward NNs for demosaicking and achieved reasonable performance. Our NN framework is expected to splendidly learn this kind of learning-based methods thanks to the strong resemblance between the two, as long as approximative sigmoid functions are bestowed.

(5) Iterative: Some state-of-the-art CFA interpolators are iterative. Gunturk et al. [17] made use of inter-channel correlation in an alternating projections scheme: Two constraint sets are defined on the basis of the observed data and the prior knowledge with respect to the correlation of the channels, and initial estimates are projected onto these constraint sets to reconstruct the channels. In our framework, the nonlinearity of neural transfer functions are counted on approximating these complicated interpolators.

(6) Composite and others: Some existing demosaicking algorithms fall into none of the five aforementioned sorts, and some affiliate to multiple sorts. For instance, Long et al. [18] devised a gradient-based adaptive NN method. Another example is the Kimmel's method [19], which combined the CHB and gradient-based interpolations in an iterative way: first-order derivatives of the green channel information are used to compute edge indicators in eight possible directions. Hues are interpolated using these edge indicators, and missing color intensities are determined according to the interpolated hues. The color channels are then updated iteratively to obey the color-ratio rule.

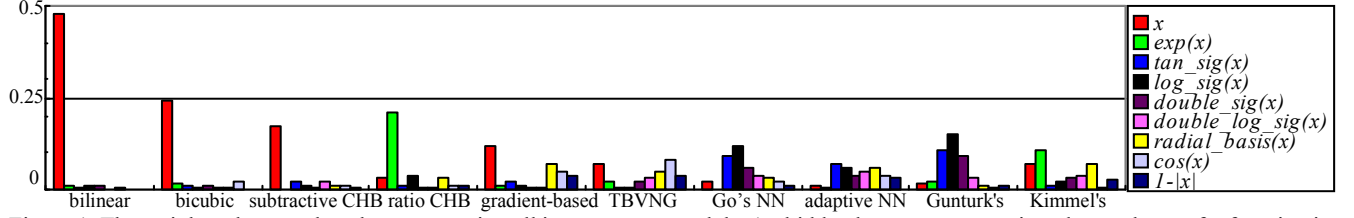


Figure 1. The weight values on the edges connecting all input neurons and the 1st hidden layer neurons assigned to each transfer function is arranged into a vector, and the L2 norms of these 9 vectors from a green channel NN for all demosaicking algorithms tested in Subsection 4.1 are visualized as the height of pillars.

3. Compositional Pattern-Producing Networks

CPPNs are a variation of NNs that differ in their set of transfer functions. While NNs typically contain only one certain type of sigmoid or radial basis functions, CPPNs can comprise a mixed configuration of both types of functions and many others. The choice of transfer functions can be biased toward specific types of patterns and regularities [20]. For instance, periodic functions like sine produce segmented patterns with repetitions; symmetric functions such as Gaussian produce symmetric patterns. Linear functions can produce linear or fractal-like patterns.

3.1. NN Topology

Basically, four-layer back propagation NNs are taken as a heuristic design specifically tailored for interpolation algorithms. The input, 1st hidden, 2nd hidden and output layers have 196, 216, 3 and 1 neuron respectively (i.e. a 196-216-3-1 topology¹). The 1st hidden layer has multiple transfer functions, each assigned a specific number of neurons: $f(x)=x$ with 1 neuron, $f(x)=exp(x)$ with 6 neurons to cancel out the logarithms of pixel values, each of $2/(1+exp(-2x))-1$, $logSig(x)=1/(1+exp(-x))$, $exp(-x)/(1+exp(-x))^2$, $sgn^2(x)(1-exp(-x^2))$, $cos(x)$, $radialBasis(x)=exp(-x^2)$, and $f(x)=max\{1-|x|,0\}$ with 30 neurons. The selected 9 transfer functions are a standard set used to approximate general high-order functions. The 2nd hidden layer has 3 transfer functions, $f(x)=x$, $logsig(x)$ and $radialBasis(x)$ for maintaining both linearity and non-linearity from the 1st layer. The transfer function of the output layer is linear.

3.2. Three Classifiers

As portrayed in Figure 1, there is obvious distinction among the distributions of weight values learnt from images demosaicked by different algorithms. Our 1st classifier Ψ_A relies on this weight space with proper PCA and multi-class SVM [21]. With a group of images interpolated by the same demosaicking algorithm d , a set of 12 NNs are trained. Then, this 12 NNs are able to simulate every pixel

of a given test image Ω , and so construct a new re-interpolated image, say Ω'_d . The more resemblant the algorithms to demosaick Ω and the group of training images, the closer to Ω is Ω'_d . Ω is categorized as being demosaicked by d , if the L1-norm of the image vector $\Omega-\Omega'_d$ is the minimum among all candidate demosaicking algorithms. This is our 2nd classifier Ψ_B . The difference map $|\Omega-\Omega'_d|$ has periodic intensity fluctuation, which manifests as particularly salient symmetric peaks in the frequency domain. Such phenomenon is quantized by the maximum of the dot products between all 5×5 patches in $DFT^3(|\Omega-\Omega'_d|)$ and the kernel $[1,2,4,2,1][1,2,4,2,1]^T$, which is the metrics of our 3rd classifier Ψ_C . Ω is categorized as being demosaicked by d , if this metrics give the maximum value among all candidate image interpolation algorithms.

The classification from Ψ_A , Ψ_B and Ψ_C for each color channel is integrated into a global decision by the Majority-Voting Scheme (MVS) [22].

4. Experimental Results

In each item of experiments, 10 images with resolution 800×600 are used, in order to learn the DIPC from a specific demosaicking algorithm via a set of 12 NNs. Since our framework is pixel-based, that is, every pixel constitutes a training sample, a single high dynamic range image is essentially enough for training. Unlike those feature-based approaches, it does not suffer the problem of compressing useful spatial information in the process of statistical accumulation, such as building histograms or correlograms. After learning the DIPC, 50 images also with resolution 800×600 is used to test the recognition rate. There are totally $10+50=60$ images for each demosaicking algorithm / super-resolution algorithm / camera. Because no NN is to learn from non-demosaicked images, only 50 non-demosaicked images are needed for test.

According to the statistics of running time for 100 times, it takes $201.3(\text{mean})\pm 12.2(\text{standard deviation})$ seconds to train one NN on a personal computer with Intel T5250 dual core 1.5G $\times 2$ CPU. For the purpose of digital photo authentication and forgery detection, recognition accuracy, reliability and robustness is the key. Provided that a proposed algorithm can always complete within a reasonable amount of time (typically several minutes) on a contem-

¹ Other NN topologies with similar size only lead to slight performance difference. To investigate the optimal topology is a purely machine learning problem, not the main aim of this work.

² $sgn(x)$ denotes the sign function. $sgn(x)=0$ for $x=0$; $sgn(x)=x/|x|$ for $x\neq 0$.

³ DFT stands for the magnitude of Discrete Fourier Transform.

porary personal computer, the computational cost should be deemed as acceptable. And the computational load would be reduced if incorporating the most recent research results by Castillo et al. [23], who proposed an improved NN training algorithm and claimed to be much faster than the Scaled Conjugate Gradient method [24].

As delivered in the subsections, this framework is not only a simple classifier, but also reveals a systematic series of traces hidden inside images induced by demosaicking.

4.1. Artificially Demosaicked Images

Table 1. Confusion matrix of demosaicking recognition

Abbreviations due to the limited space: NonD : Non-Demosaicked, BiLi : BiLinear, BiCb : BiCubic, sCHB : subtractive CHB, rCHB : ratio CHB, Grdt : Gradient[14], TBV : TBVNG[15], GoNN : Go's NN[16], adNN : adaptive NN[18], Gunt : Gunturk's[17], Kiml : Kimmel's[19]

	NonD	BiLi	BiCb	sCHB	rCHB	Grdt	TBV	GoNN	adNN	Gunt	Kiml
NonD	96	0	0	0	0	0	2	0	0	0	2
BiLi	0	100	0	0	0	0	0	0	0	0	0
BiCb	0	2	98	0	0	0	0	0	0	0	0
sCHB	0	0	2	96	0	2	0	0	0	0	0
rCHB	0	0	0	0	90	0	2	0	0	2	6
Grdt	0	0	0	2	0	96	2	0	0	0	0
TBV	2	0	0	0	0	6	88	0	4	0	0
GoNN	0	0	0	0	0	0	2	98	2	0	0
adNN	0	0	0	0	0	2	4	92	0	0	0
Gunt	2	0	0	0	2	0	0	0	0	94	2
Kiml	0	0	0	0	4	6	0	0	0	2	88

Images demosaicked by the 10 algorithms mentioned in Section 2 and the non-demosaicked ones form 11 classes of images. No NN learns the DIPC of non-demosaicked images; instead, it is identified when a rejection arises from the MVS. Table 1 shows the resulted confusion matrix.

4.2. Photos Produced by Commercial Cameras

Table 2. Confusion matrix of source camera identification

NonD:Non-Demosaicked, DEC:DEC U350, SP73:Sony P73, ST10:Sony T10, Koda:Kodak Z730, Can.:Canon A470, Niko:Nikon L18, Rico:Ricoh R50, Casio:Casio EX-Z9, Sams:Samsung S860, Olym:Olympus IS5000

	NonD	DEC	SP73	ST10	Koda	Can.	Niko	Rico	Casio	Sams	Olym
NonD	94	0	0	0	2	0	2	0	0	2	0
DEC	0	96	2	0	0	0	0	0	0	0	2
SP73	0	2	84	8	0	4	0	2	0	0	0
ST10	0	0	6	88	0	2	0	2	2	0	0
Koda	2	0	0	0	90	0	2	0	0	2	4
Can.	0	0	2	2	0	92	4	0	0	0	0
Niko	2	0	2	0	2	6	86	0	2	0	0
Rico	0	0	2	2	2	0	0	94	0	0	0
Casio	0	0	0	0	2	0	2	0	88	4	4
Sams	4	0	0	0	2	0	0	0	2	92	0
Olym	0	4	0	0	2	0	0	0	4	0	90

The efficacy of our method is also tested on photos produced by 10 commercially available digital cameras: DEC U350, Sony P73, Sony T10, Kodak Z730, Canon A470, Nikon L18, Ricoh R50, Casio EX-Z9, Samsung S860 and Olympus IS5000. All cameras are set to store photos in uncompressed format. A class of cartoon pictures

is added as non-demosaicked images. As demonstrated in Table 2, the loss in recognition rate is clear, compared to that on ideal demosaicking operators in Subsection 4.1. This is natural considering the fact that, noise engendered in various stages of the image formation pipeline of a digital camera more or less destroys the periodic DIPC.

4.3. Super-Resolution Algorithms Recognition

Table 3. Confusion matrix of SR algorithm recognition

Origin:Original, Re:Replicate, BL:BiLinear, BC:BiCubic, HN:Hybrid NN

	Origin	Re2X	BL2X	BC2X	HN2X	Re3X	BL3X	BC3X	HN3X	Re4X	BL4X	BC4X	HN4X
Origin	98	0	0	0	2	0	0	0	0	0	0	0	0
Re2X	0	92	0	0	2	0	0	0	0	6	0	0	0
BL2X	0	0	86	2	0	0	2	0	0	0	8	0	2
BC2X	0	0	0	84	4	0	0	0	0	0	0	10	2
HN2X	2	0	0	6	80	0	0	0	4	0	0	0	8
Re3X	0	0	0	0	0	100	0	0	0	0	0	0	0
BL3X	0	0	0	0	2	0	94	0	0	0	2	0	2
BC3X	0	0	0	0	0	0	0	98	0	0	0	0	2
HN3X	2	0	0	0	4	0	0	0	90	0	0	0	4
Re4X	0	10	0	0	0	0	0	0	0	90	0	0	0
BL4X	0	0	14	0	0	0	2	0	0	0	82	0	2
BC4X	0	0	0	12	0	0	0	2	2	0	0	82	2
HN4X	0	0	4	0	8	0	0	0	6	0	4	0	78

Lately it has been disclosed that Super-Resolution (SR) and demosaicking are two faces of the same problem and it is rational to address them in a unified context [25]. Unlike demosaicking, the spatial period along x/y axis may be an arbitrary real number depending upon the magnification ratio. We are still trying to retrieve DIPC if the exact spatial period is barely known. At present, recognition among 4 SR algorithms, pixel replication, bilinear, bicubic spline and a hybrid NN-based SR [26], is implemented provided that, the same SR algorithm with varying magnification ratios is reckoned as dissimilar algorithms. 2X, 3X and 4X SRs have 4, 9 and 16 distinct spatial phases respectively, each lying on a set of $4 \times 3 = 12$, $9 \times 3 = 27$ and $16 \times 3 = 48$ NNs for all 3 color channels of a whole image. Table 3 is the resultant confusion matrix.

4.4. Digital Photo Authentication

Photo authentication is the core item of experiments. The metrics of Ψ_B and Ψ_C are excellent indicators to expose faked photos: Figure 2 is an image containing perceptually plausible forgeries created using Adobe Photoshop with the suspicious regions framed, and their corresponding difference map $|\Omega - \Omega'|$ for Ψ_B and the Fourier transformed suspicious framed windows in $|\Omega - \Omega'|$ for Ψ_C . The real photo, from which the fabrication is made, are shot by the DEC U350 camera. The Ψ_B metrics i.e. the L1-norms of the suspicious framed windows in $|\Omega - \Omega'|$ augment from 35947 to 81037, and the Ψ_C metrics i.e. the kernel-dot-product maximum diminishes from 17144 to 8347.

4.5. DIPC Impairment and Transfer

The DIPC signal pattern plays the role of a signature, that is, it acts like a peculiar watermark unique to each CFA

interpolation algorithms. This enlightens us to follow the rationale of watermark estimation, weakening / copy attack [27] using the Wiener filter [28]: In this understanding, the test image Ω is the watermarked signal. Suppose DIPC watermark complies with Laplacian distribution, the Maximum Likelihood estimate of the original signal Φ has a closed form solution given by the local median of the watermarked signal [27]. This coincides with the findings in [8] that, DIPC is vulnerable to median filtering. Let Ω' be the re-interpolated image by its recognizable NNs. $\Omega'-\Phi$ is the estimated ideal watermark that should have the same vibration direction but larger amplitude with the real watermark $\Omega-\Phi$ i.e. $|\Omega'-\Phi|>|\Omega-\Phi|$, $(\Omega'-\Phi)(\Omega-\Phi)>0 \Rightarrow \Omega'<\Omega<\Phi$ or $\Omega'>\Omega>\Phi$. If the inequality does not hold at (x,y) , either Ω' or Φ is incorrectly estimated at this pixel location, and (x,y) is left unaltered; otherwise Ω is updated to be $\Omega+k(\Phi-\Omega)$ where $k=\sigma/T$ when the local variance σ is less than the threshold T , $k=1$ when $\sigma>=T$. Likewise, in DIPC transfer, Ω is updated toward Ω' to be $\Omega+k(\Omega'-\Omega)$. Figure 3 illustrates an example where it is seen that, DIPC is effectually removed or copied while image detail information is well preserved.

5. Concluding Remarks and Future Work

Huang [29] theoretically showed that any direct forgery detection can be cracked by an anti-detection algorithm specially designed against it. Howbeit investigating statistical characteristics inherent in digital photos is still an active and promising field, since most counterfeit photos to be inspected are produced without the post-processing of all anti-detection algorithms.

An interesting problem for potential future work is that, all contemporary DIPC-based methods for digital forensics including ours, assume that a camera will use certain kind of fixed demosaicking algorithm throughout the whole image. No previous methods attempt to handle images adaptively interpolated by different demosaicking algorithms over either spatial or frequency domain. However, some cameras may apply different demosaicking algorithms to different portions of the image depending on the natural statistics of the image content and image patch scene correlation. In such circumstances, all proposed approach will misjudge these images as tampered because different regions of the images have different DIPC.

6. References

- [1] S.Bayram, I.Avcibas, B.Sankur, and N.Memon, Image manipulation detection, *Journal of Electronic Imaging*, 15(4): 041102, 2006.
- [2] H.Farid, A survey of image forgery detection, *IEEE Signal Processing Magazine*, 26(2): 16-25, 2009.
- [3] M.Kharrazi, H.T.Sencar, and N.Memon, Blind Source camera identification, *Proceedings of IEEE International Conference on Image Processing 2004*, pp.709-712.
- [4] S.Bayram, H.Sencar, N.Memon, and I.Avcibas, Source camera identification based on CFA interpolation, *Proceedings of IEEE International Conference on Image Processing 2005*, pp.69-72.
- [5] A.C.Popescu, and H.Farid, Exposing digital forgeries in color filter array interpolated images, *IEEE Transactions on Signal Processing*, 53(10): 3948-3959, 2005.
- [6] O.Celiktutan, B.Sankur, and I.Avcibas, Blind identification of source cell-phone model, *IEEE Transactions on Information Forensics and Security*, 3(3): 553-566, 2008.
- [7] Y.J.Long, and Y.Z.Huang, Image based source camera identification using demosaicking, *Proceedings of the 8th International Workshop on Multimedia Signal Processing*, pp. 419-424, 2006.
- [8] Y.Z.Huang, and Y.J.Long, Demosaicking recognition with applications in digital photo authentication based on a quadratic pixel correlation model, *Proceedings of CVPR 2008*, pp.1-8.
- [9] A.Swaminathan, M.Wu, and K.J.Ray Liu, Non-intrusive component forensics of visual sensors using output images, *IEEE Transactions on Information Forensics and Security*, 2(1): 91-106, 2007.
- [10] N.Fan, C.Jin, and Y.Z.Huang, A pixel-based digital photo authentication framework via demosaicking inter-pixel correlation, *Proceedings of ACM Multimedia and Security Workshop 2009*, pp.125-130.
- [11] B.Gunturk, J.Glotzbach, Y.Altunbasak, R.Schafer, and R.Mersereau, Demosaicking: Color filter array interpolation in single-chip digital cameras, *IEEE Signal Processing Magazine*, 22(1): 44-54, 2005.
- [12] B. E. Bayer, Color imaging array, U.S. Patent, No. 3,971,065, 1976.
- [13] D.R.Cok, Signal processing method and apparatus for producing interpolated chrominance values in a sampled color image signal, U.S. Patent, No. 4,642,678, 1986.
- [14] C.A.Laroche, and M.A.Prescott, Apparatus and method for adaptively interpolating a full color image utilizing chrominance gradients, U.S. Patent, No. 5,373,322, 1994.
- [15] E.Chang, S.Cheung, and D.Y.Pan, Color filter array recovery using a threshold-based variable number of gradients, *SPIE vol. 3650*, pp. 36-43, 1999.
- [16] J.Go, K.Sohn, and C.Lee, Interpolation using neural networks for digital still cameras, *IEEE Transactions on Consumer Electronics*, 46(3): 610-616, 2000.
- [17] B.Gunturk, Y.Altunbasak, and R.Mersereau, Color plane interpolation using alternating projections, *IEEE Transactions on Image Processing*, 11(9): 997-1013, 2002.
- [18] Y.J.Long, and Y.Z.Huang, Adaptive demosaicking using multiple neural networks, *Proceedings of IEEE International Workshop on Machine Learning for Signal Processing 2006*, pp.353-357.
- [19] R.Kimmel, Demosaicking: Image reconstruction from CCD samples, *IEEE Transactions on Image Processing*, 8(9): 1221-1228, 1999.
- [20] K.O.Stanley, Compositional pattern producing networks: A novel abstraction of development, *Genetic Programming and Evolvable Machines*, 8(2): 131-162, 2007.
- [21] C.W.Hsu, and C.J.Lin, A comparison of methods for multi-class support vector machines. *IEEE Transactions on Neural Networks*, 13: 415-425, 2002.
- [22] L.Lam, and C.Y.Suen, Application of majority voting to pattern recognition: An analysis of its behavior and perfor-

mance, IEEE Transactions on Systems, Man and Cybernetics, 27(5): 553–568, 1997.

- [23] E.Castillo, B.G.Berdinas, O.F.Romero, and A.A.Betanzos, A very fast learning method for neural networks based on sensitivity analysis, Journal of Machine Learning Research, 7: 1159-1182, 2006.
- [24] A.F.Moller, A scaled conjugate gradient algorithm for fast supervised learning, Neural Networks, 6(4): 525-533, 1993.
- [25] Sina Farsiu, Michael Elad, Peyman Milanfar, Multi-frame demosaicing and super-resolution of color images, IEEE Transactions on Image Processing, 15(1): 141-159, 2006.
- [26] Y.Z.Huang, and Y.J.Long, Super-resolution using neural

networks based on the optimal recovery theory, Journal of Computational Electronics, 5(4): 275-281, 2006.

- [27] M.Kutter, S.Voloshynovskiy, and A.Herrigel, The watermark copy attack, SPIE vol. 3971, Security and Watermarking of Multimedia Contents II 2000, pp.371-380.
- [28] N.Wiener, Extrapolation, interpolation, and smoothing of stationary time series, John Wiley & Sons, NY, 1949.
- [29] Y.Z.Huang, Can digital image forgery detection unevadable? A case study: Color filter array interpolation statistical feature recovery, SPIE vol. 5960, Visual Communications and Image Processing 2005, pp.980-991.

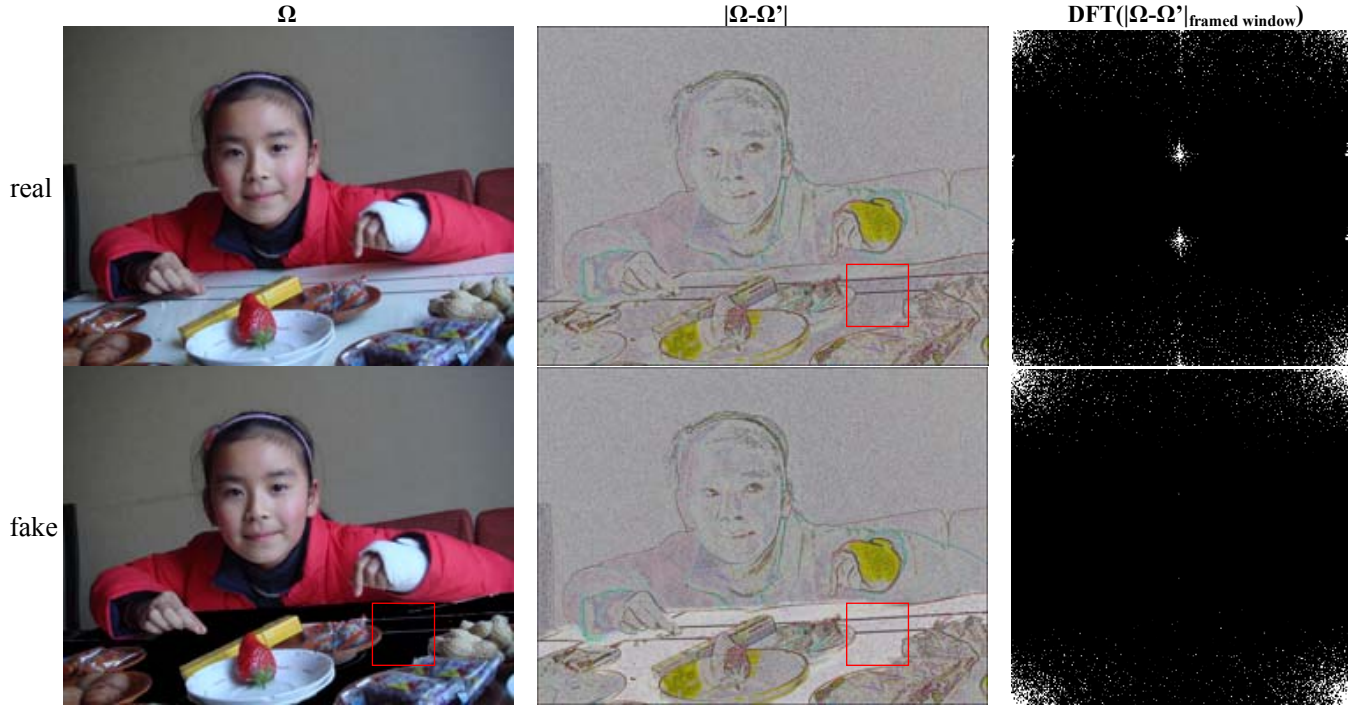


Figure 2. A forgery detection example: The three columns, from left to right, are the test image Ω , the difference map $|\Omega-\Omega'|$, and the magnitude of the Fourier transform of the suspicious framed windows in $|\Omega-\Omega'|$ respectively. Exceptional highlight in $|\Omega-\Omega'|$ and the absence of evident peaks in spread spectrum over the framed windows in $|\Omega-\Omega'|$ displays the corruption of DIPC, directing forged areas.



Figure 3. The first and second row is an example of DIPC impairment and transfer respectively. In each line, 6 images from left to right are an original image, a modified images, their corresponding difference map $|\Omega-\Omega'|$, and Fourier transformed $|\Omega-\Omega'|$.